INORGANIC CHEMISTRY FRONTIERS

RESEARCH ARTICLE

View Article Online
View Journal | View Issue

Cite this: *Inorg. Chem. Front.*, 2023, **10**, 5082

Fast rotating dipole array inducing large dielectric response in a Ruddlesden–Popper hybrid perovskite ferroelastic†

Wang Luo,‡[a] Na Wang,‡[a] Hua-Kai Li,[a] Ze-Jiang Xu,[a] Yan Feng,[a] Xiao-bin Fu, *[b] Chao Shi, *[a] Heng-Yun Ye [a] and Le-Ping Miao *[a]

Received 30th May 2023,
Accepted 21st July 2023

DOI: 10.1039/d3qi01000g

rsc.li/frontiers-inorganic

Dynamic functional materials have attracted increasing interest owing to their broad potential applications in the field of flexible smart. Molecular rotors are a good platform to achieve functionality because of the intrinsic movement of the internal components. Herein, we report a two-dimensional (2D) Ruddlesden–Popper (RP) type hybrid perovskite ferroelastic $(TFCA)_2CdCl_4$ (**1**; TFCA = 2-fluoro-1-amino-pyrrolidium) showing T_c (402 K) and spontaneous strain (0.071). Impressively, the rapid rotating motions of the polar rotors lead to the fast reorientation of the dipoles resulting in a large dielectric response. The switching on–off ratio of dielectric anomaly is more than 100 ($\varepsilon'_{HTP}/\varepsilon'_{LTP} > 100$) at a high-frequency electric field (1 MHz). This study reveals that the 2D RP hybrid perovskite molecular rotor platform provides a new avenue to explore dynamic functional materials.

Introduction

In recent decades, ferroic materials (ferroelectric, ferromagnetic, and ferroelastic) have received unprecedented attention owing to their broad applications in the fields of information storage, signal conversion, energy conversion, and other intelligent devices.[1–3] Ferroelasticity is a mechanical simulation of ferroelectric and ferromagnetic properties. Under the stimulation of a force field they exhibit spontaneous lattice strains, ferroelastic domain evolution, and mechanical twinning.[4,5] This characteristic property of ferroelastic materials results in huge potential applications in force-sensitive devices, such as shape memory, sensors, and mechanical switches.[6–8] To the best of our knowledge, the structural phase transitions (SPT) triggered by the dynamic concerted movement of the internal molecules is the key element in obtaining ferroelasticity.[9,10] Ferroelastics usually show a ferroelastic phase emergence in a lower-symmetric phase *via* a symmetry-breaking during the SPT.[11–13] This means the ferroelastics require changes in symmetry. Hence the design of ferroelastic materials still faces challenges. Especially, the molecular-level origin of ferroelasticity is yet to be fully understood.

In the dynamic molecular structural family, there is a specific kind of crystal with intrinsic molecular motions, namely molecular rotors.[14,15] These kinds of amphidynamic crystals consist of dynamic rotators and relative static stators at a molecular level. The intrinsic motions of the arrayed rotors result in cooperative molecular interactions to activate SPT.[16,17] Moreover, the rotary motions of rotors are commonly associated with switching macroscopic physical properties, such as ferroicity and dielectric transition.[12,18–23] In particular, the rapid rotating movement of rotors means the fast reorientation of dipoles, which can induce large dielectric responses.[24,25] Therefore, molecular rotor structures are a promising platform to realize new dynamic functional properties. However, the construction of the rotor-stator-type structures in a crystalline state remains a challenge.

Organic–inorganic hybrid perovskites have been widely used to build dynamic structures owing to the advantages of easy synthesis, easy derivation, and adjustable structures benefitting to achieve the order–disorder movement.[26,27] The two-dimensional (2D) organic–inorganic hybrid perovskites (OIHPs) are good representative[28–30] because they have the unique host–guest dynamic structural model that causes organic guest cations to be thermally driven into an order–disorder movement in the interlayer of the inorganic rigid host-framework. Simultaneously, the relevant molecular motion can induce SPT, further obtaining ferroelasticity.[31,32] In particular, the Ruddlesden–Popper (RP) type 2D hybrid perovs-

[a]*Chaotic Matter Science Research Center, Metallurgy and Chemistry, Jiangxi University of Science and Technology, Ganzhou 341000, China. E-mail: miaoleping@jxust.edu.cn*
[b]*Department of Molten Salt Chemistry and Engineering, Shanghai Institute of Applied Physics, Chinese Academy of Sciences, Shanghai, 201800, China*

†Electronic supplementary information (ESI) available. CCDC 2265824 and 2265825. For ESI and crystallographic data in CIF or other electronic format see DOI: https://doi.org/10.1039/d3qi01000g

‡These authors contributed equally.

kites exhibit a higher probability to achieve SPT due to the van der Waals (vdW) layers.[33–35] This is because the vdW layers denote the weak interactions between the tightly packed organic cations reducing the motional energy barrier required for SPT.[36–38]

Therefore, combining the 2D RP hybrid perovskites and a molecular rotor will provide a new avenue to realize ferroicity and a large dielectric anomaly response (Scheme 1). Herein, we designed a 2D RP hybrid perovskite ferroelastic crystal **1** [$(TFCA)_2CdCl_4$] (TFCA = 2-fluoro-1-amino-pyrrolidium) with a characteristic molecular rotator structure. It consists of hydrogen-bonded polar organic rotors and inorganic layered stators. The variable temperature X-ray diffraction crystal structure and solid-state nuclear magnetic resonance (ss-NMR) spectra reveal that the thermal-driven fast rotation of the polar rotor triggers the ferroelasticity of **1**. Meanwhile, the fast dynamics of the dipoles result in a large dielectric switching response ($\varepsilon'_{HTP}/\varepsilon'_{LTP} > 100$ at 1 MHz). This study provides a new platform for building novel molecular rotor functional materials.

Results and discussion

Structural phase transition

Compound **1** is a transparent plate crystal prepared by the slow evaporation of the clarified aqueous solution (Fig. S1†). The powder X-ray diffraction (PXRD) patterns confirm the pure phase of crystal **1** (Fig. 1a). In addition, thermogravimetry (TG) was used to evaluate the thermal stability of **1**. The results are shown in Fig. S2,† indicating that this hybrid molecular crystal is stable up to 443 K. The reversible structural phase transition (SPT) of **1** was preliminarily confirmed by differential scanning calorimetry (DSC) measurements (Fig. 1b). There is an obvious pair of endothermic/exothermic peaks around 402/369 K during the heating/cooling process. This proves the true SPT of **1**. Besides, the thermal hysteresis (33 K) indicates that the SPT of **1** has the characteristics of first-order phase transition.

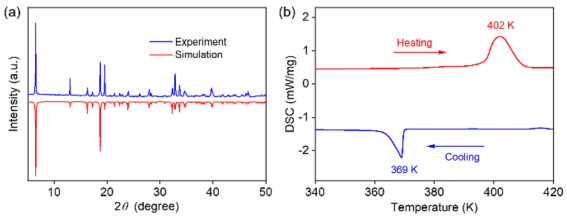

Fig. 1 (a) PXRD patterns of **1** at 293 K. (b) DSC curves of **1** at 340–420 K.

Crystal structures

In order to reveal the mechanism of the SPT, the crystal structures of **1** at 323 K and 423 K were collected and analyzed. In general, this hybrid molecule crystal belongs to a two-dimensional (2D) RP hybrid perovskite structure in which the octahedral 2D inorganic layer is constructed by anions (Cl^-) and metal ions (Cd^{2+}). Cationic TFCA rotor arrays with a van der Waals layer are located in the interlamination of the 2D layer (Fig. S3†). In addition, the 2D inorganic anion framework is formed through angular shared $[CdCl_6]^{4-}$. Besides, the organic cation rotors occupy the cavities constructed by the slightly twisted octahedron through hydrogen bond interactions.

In the low-temperature phase (LTP) 323 K, **1** crystallizes in the orthomorphic system (*Pbcn* space group) with a cell parameter of a = 8.3356(4) Å, b = 7.5132(4) Å, c = 27.2065(12) Å, V = 1703.86(14) $Å^3$ (Table S1†). TFCA cations are fixed in a twisted 2D anionic inorganic layer by hydrogen bonding (Fig. 2a). The static TFCA formed three kinds of hydrogen bonds with chlor-

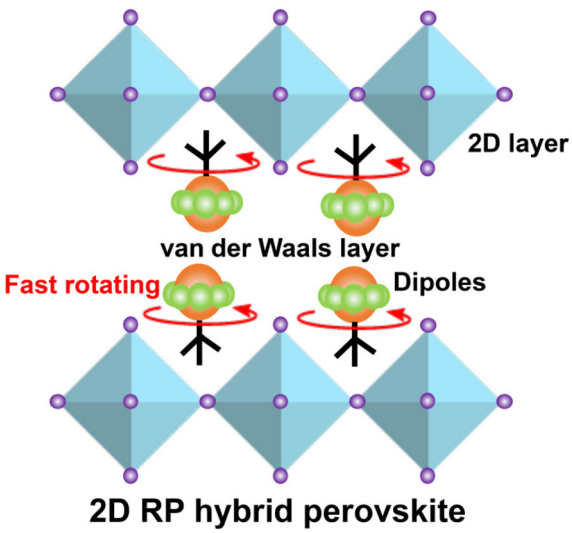

Scheme 1 The design of a 2D RP hybrid perovskite molecular rotor with fast-rotating dipoles.

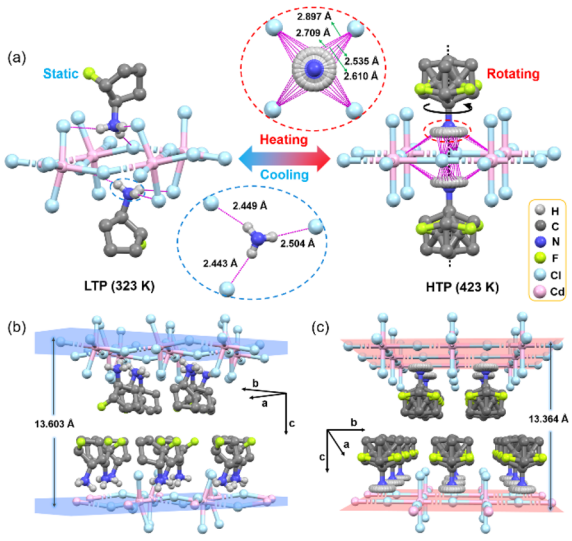

Fig. 2 (a) Dipole rotor TFCA reorientation and interaction changes of **1** between 323 K (LTP) and 423 K (HTP). (b and c) The molecular structural packing model in LTP and HTP of **1** (some of the hydrogen atoms have been omitted for clarity).

ide ions along specific directions. And the lengths of the hydrogen bond are 2.443, 2.449, and 2.504 Å (Fig. 2a). In the high-temperature phase (HTP) 423 K, molecular rotor **1** transforms into a tetragonal system (*I*4/*mmm* space group) with a cell parameter of a = 5.8052(10) Å, b = 5.8052(10) Å, c = 26.729 (4) Å, V = 900.8(2) Å^3. The interactions between TFCA and the 2D anion framework change with the rotation of the dipole rotors. It leads to four kinds of hydrogen bonds with distances of 2.535, 2.610, 2.709, and 2.877 Å (Fig. 2a). These results indicate that the polar rotor rotates around the axis of the –NH_3^+ group (Fig. 2a). In addition, the anionic framework also displays obvious changes. In LTP, the anionic framework constructed by Cd^{2+} and Cl^- is a distorted 2D layer. The angles between Cd–Cl–Cd inside the 2D layer are 161.72°, 83.04°, and 99.50° (Fig. S4†). Besides, the two chloride ions outside the 2D layer are not perpendicular to the 2D plane. And the angles of Cl3–Cd2–Cl4 and Cl5–Cd3–Cl6 are 98.89° and 98.79°, respectively. In fact, all Cl–Cd–Cl in the octahedron are not equal to 90° (Table S2†). When in HTP, the 2D framework becomes a fully regular octahedral array, with all Cl–Cd–Cl angles of 90° (Fig. S4†). More interestingly, an anomalous change is the decrease of the distance between the 2D inorganic layers from 13.603 to 13.364 Å (Fig. 2b and c), which should be attributed to the changes in the interactions between the polar rotor and the 2D inorganic layers. It is observed by the weakened N–H···Cl hydrogen bond between TFCA and inorganic 2D layers in HTP (Tables S3 and S4†). In short, variable temperature single crystal structures of **1** reveal that the fast motions of TFCA and the 2D anion framework distortion are the molecular origins of SPT.

Dynamics of the polar rotor

The variable temperature single-crystal structures show that the orientation of TFCA cations changes with temperature. The dynamics of polar rotors was analyzed using the variable temperature ss-NMR method. First, the ^{1}H–^{13}C CP/MAS NMR spectra were performed for the polar rotor TFCA. At 300 K, four signals could be observed at 23.5, 32.5, 59.8, and 97.5 ppm. These correspond to C1–C5 (C2 and C5 are the same signals) in the dipole rotor (Fig. 3a and b). No obvious changes could be observed below 380 K, which indicates that the molecular motion remains unchanged. When the temperature rises to 400 K, the signals greatly weakened and almost disappeared at 420 K. In the ^{1}H–^{13}C CP/MAS NMR method, signal intensity is based on the ^{1}H–^{13}C dipolar interactions. In fact, the dipole interactions could be suppressed by the fast dynamics of the detected atom pairs. Thus, the disappearance of the signals at 400 K illustrates the fast dynamics of the polar rotors corresponding to the previous experimental results. In addition, the ^{13}C single pulse excitation (SP/MAS) NMR method was also performed to check the dynamics of the rotors. The ^{13}C SP/MAS NMR spectra were shown in Fig. 3c. Almost no signals of the ^{13}C atoms could be observed at low temperatures (below 380 K). The absence of the ^{13}C signals should be due to the long spin–lattice relaxation (T_1 relaxation) and the short recycle delay time (D1 = 2 s) used in the experiments. As the temperature rises to 400 K, the intensity of C3, C1, and C2/C5 signals are extremely enhanced and finally turned into strong and narrow signals. The increase in the signal intensity accounted for the decrease in the ^{13}C T_1 relaxation time.[39] According to Bloembergen–Purcell–Pound (BPP) theory, the molecular motion is comparable to the T_1 relaxation time.[40] Thus, the decrease of ^{13}C T_1 relaxation time indicates the fast dynamics of the ^{13}C atoms. This result indicates that the polar rotors have a fast motion at high temperatures. Notably, the signals of C4 show no obvious changes during the whole range from 300 K to 420 K, indicating that the C4 atom should be in a relatively immobile state. Thus, the solid-state NMR results reveal that the polar rotors rotate fast around the axis of the N–C4 bond (Fig. 3a), which matches the disordering state of the single-crystal structure.

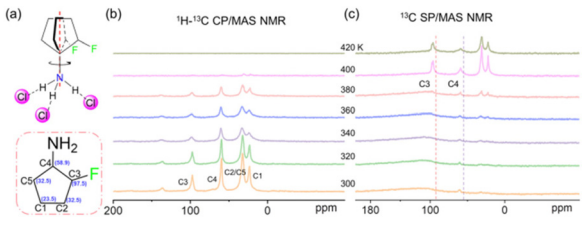

Fig. 3 (a) The rotating motion mode and C atoms naming and corresponding chemical shift of polar rotor TFCA. (b)^{1}H–^{13}C CP/MAS NMR spectra of **1** around 300–420 K. (c) ^{13}C SP/MAS NMR spectra of **1** at the range of 300–420 K.

Dielectric response

The local freezing and rotation of polar components under heat stimuli induce changes in macroscopic physical properties, such as dielectric constant, which are designed for dynamic functional materials.[3,10,24] The dielectric constant can be expressed as, $\varepsilon_r = \varepsilon' - i\varepsilon''$, where ε' and ε'' represents the real part and imaginary part, respectively. Thus, we performed the temperature-dependent changes of the dielectric constant at the range of 320–430 K. The real and imaginary parts of the dielectric constant show large stepped and λ-like anomalies, respectively, confirming the rotating motion of the polar dipoles (Fig. 4a and b). In addition, the ε' and ε'' values decreased with increasing frequency (0.5, 1, 5, 10, 100 kHz, and 1 MHz), indicating that the permittivity of compound **1** was frequency-dependent. More importantly, **1** displayed an extremely large dielectric switching response. In the high frequency of 1 MHz, the ε' value was greater than 700 in the HTP and less than 7 in the LTP (Fig. 4c). In other words, compound **1** has a large dielectric switching ratio, $\varepsilon'_{HTP}/\varepsilon'_{LTP} > 100$, which is extremely rare among 2D organic–inorganic hybrid ferroelastics because most of them exhibit low dielectric responses ($\varepsilon'_{HTP}/\varepsilon'_{LTP} < 50$) (Table 1).[39–57] According to the fundamental dielectric theories, the dielectric response depends on the molecular structure, temperature, and the frequency of the electric field when an AC field is applied. In fact, the orientation of molecular dipoles is slower compared to the distortional polarization (relative displacement/deformation of

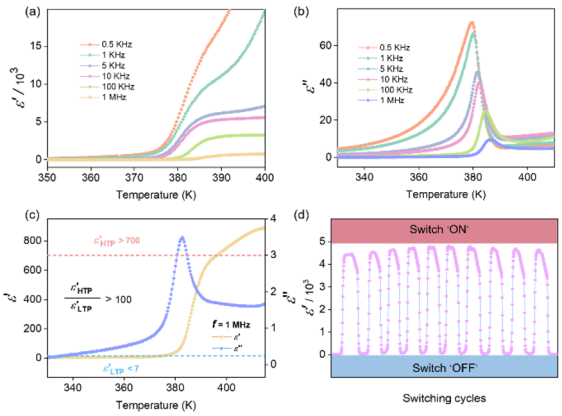

Fig. 4 The dielectric anomaly measurement of polycrystalline samples of **1**. (a) ε' at different frequencies upon heating. (b) ε'' at different frequencies upon heating. (c) ε' and ε'' at 1 MHz. (d) After 10 switching cycles at a frequency of 25 kHz, the value of the dielectric constant shows a sensitive switchable with no decrease.

Table 1 The comparison of dielectric switching ratio at 1 MHz between ferroelastic **1** and the selected 2D organic–inorganic perovskites

Formula[a]	$\varepsilon'_{HTP}/\varepsilon'_{LTP}$	Ref.
$(C_3H_5CH_2NH_3)_2[MnCl_4]$	<2	41
$[C_5H_9NH_3]_4Cd_3Cl_{10}$	<2	42
$(IAA)_2PbCl_4$	<2	43
$[2,5\text{-DCA}]_2\cdot[CuCl_4]$	<2	44
$(N\text{-Methylcyclohexylaminium})_4Pb_3I_{10}$	<2	45
$[C_4H_9N]_2[PbBr_4]$	<2	46
$[3,3\text{-Difluorocyclobutylammonium}]_2CuCl_4$	<2	47
$(R\text{-3AMP})PbBr_4$	<2	48
$(DPA)_4AgBiBr_8$	<2	49
$(N\text{-Methylcyclohexylaminium})_4Pb_3I_{10}$	<2	50
$(EA)_4Pb_3Cl_{10}$	<5	41
$(C_4H_9NH_3)_2PbCl_4$	<6	52
$NH_3(CH_2)_5NH_3MnCl_4$	<6	53
$(PEA)_2CdCl_4$	<6	54
$(HQ)_4KEu(NO_3)_8$	<8	55
$(EATMP)PbBr_4$	<8	56
$(R3HQ)_4KCe(NO_3)_8$	<10	57
$[Br(CH_2)_3NH_3]_2PbBr_4$	<20	58
$(4,4\text{-Difluoropiperidinium})_4AgBiI_8$	<45	59
$(TFCA)_2CdCl_4$	>100	This work

[a] IAA = isoamylammonium cation; 2,5-DCA = 2,5-dichloroamylamine; 3AMP = 3-(aminomethyl)-piperidine; DPA = 2,2-dimethylpropan-1-aminium; EA = ethylammonium; PEA = phenethylamium cation; HQ = quinuclidine; EATMP = (2-aminoethyl)-trimethylphosphanium; EATMP = (2-aminoethyl)trimethylphosphanium; R3HQ = *rac*-3-hydroxylquinuclidinium; TFCA = 2-fluoro-1-amino-pyrrolidium.

charges under the action of an electric field). As a result, the achieved polarization is incomplete and uniform due to the interference of the thermal motion. This means that the dielectric response will reach an equilibrium state when the electric field is applied for a long time (low frequency). Then the dielectric permittivity accomplishes its maximum value corresponding to the maximum polarization.[60] In contrast, in high-frequency electric fields, there is no necessary time for the reorientation of dipoles. Thus, polarization only contains the contribution of distortional effects resulting in a low value of dielectric permittivity. Therefore, crystal **1** displaying a large dielectric anomaly around T_c even at a high frequency (1 MHz) should be attributed to the fast thermal driven free rotary motions of the fluoro-substituted polar dipole rotor.[14,24] This is because the fast dynamics of dipoles means the dipoles reorientation could match with the external electric field frequency resulting in a large dielectric response. In short, these reveal that a 2D RP hybrid perovskite with a van der Waals layer combing fast rotating polar rotors is an effective avenue to achieve a large dielectric anomaly. Further, the dielectric switch of compound **1** was investigated by repeated heating/cooling, *i.e.* the transition between high dielectric states (switch "ON") and low dielectric states (switch "OFF"). As shown in Fig. 4d, the temperature-triggered dielectric switch can be switched sensitively near the T_c and the value of dielectric permittivity hardly attenuates during the 10 heating–cooling cycles. These results show that the hybrid molecule crystal **1** has a sensitive dielectric switch and excellent fatigue resistance, indicating good potential applications in the bulk capacitor dielectric materials.

Ferroelasticity

According to the changes in the symmetry of **1**, we found that this hybrid molecule may belong to a ferroelastic crystal. Because the space group change conforms to one of the 94 ferroelastic phase transitions, which can be labeled as Aizu symbol 4/*mmmFmmm*.[54,61] In fact, the orthogonal lattice of LTP is in a low symmetric ferroelastic phase with 8 symmetric elements (E; $2C_4$; C_2; $2C'_2$; $2C''_2$; i; σ_h; σ_v; σ'_v), while the tetragonal lattice of HTP is a higher symmetric paraelastic phase with 16 symmetric elements (E; $2C_4$; C_2; $2C'_2$; $2C''_2$; i; $2S_4$; σ_h; $2\sigma_v$ and $2\sigma_d$). That is the ferroelastic phase of **1** has two orienting states.[41,62] Thus, the spontaneous strain ε_s calculated for the ferroelastic phase based on cell unit parameters at 323 K (a_f, b_f, c_f) and 423 K (a_p, b_p, c_p) is 0.071 (see ESI†). This surpasses the reported 2D RP hybrid perovskites $(C_3H_5CH_2NH_3)_2[MnCl_4]$ (0.038) and $(C_3H_5CH_2NH_3)_2[CdCl_4]$ (0.036).[41] It also indicates that the molecular rotor ferroelastic crystal **1** has good potential in the field of mechanical force devices.

Ferroelastic crystals along with birefringence properties exhibit bright and dark patterns in orthogonally polarized light due to the different orientations of the ferroelastic domain. In addition, the evolutions of domains near T_c are characteristic to ferroelastic crystals. Therefore, the ferroelastic domains of the massive crystals of **1** during heating/cooling were performed through polarization optical microscopy (Fig. 5A–H). At 343 K, the morphology of the plate crystals of **1** is independent of its ferroelastic domains with clear crisscross ferroelastic domain structures under polarized light (Fig. 5A and B). Furthermore, during the heating and cooling process, the ferroelastic domains present dynamic changes. When the temperature rises to T_c, the domain structure in HTP completely disappears and the crystal morphology turns into black under polarized light (Fig. 5C and D). At the same time, the crystal morphology under natural light is consistent with LTP

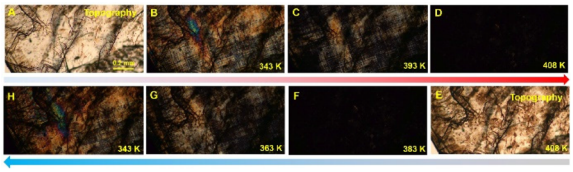

Fig. 5 Evolutions of the ferroelastic domains under the polarizing microscope. (A) Natural optical microscope image for a single crystal of **1** in LTP, (B–D) evolutions of the ferroelastic domain structure for **1** in the heating, (E) natural optical microscope image for single crystal **1** in HTP, (F–H) and ferroelastic domain evolutions of **1** in the cooling process.

(Fig. 5E). The ferroelastic domain structure reappeared when the temperature cooled below T_c. Furthermore, the domain structure gradually increased and became clear and bright with the decrease in temperature (Fig. 5F and H). In addition, the ferroelastic domain evolution during two cycles of heating/cooling is completely recorded by the video showing the completely reversible evolution process (ESI movie†). These pieces of evidence reveal that **1** is a ferroelastic crystal, indicating its potential applications in force-sensitive devices, such as actuators.

Conclusions

In summary, we designed a 2D RP organic–inorganic hybrid perovskite with vdW layers of weak molecular interactions as a platform for constructing molecular rotor material. In addition, the thermal-driven fast-rotating motion of the polar rotors induces ferroelasticity. Remarkably, the rapid rotary motion of the dipolar rotor is accompanied by a large dielectric response that causes a dielectric switching on–off ratio of more than 100 ($\varepsilon'_{HTP}/\varepsilon'_{LTP} > 100$ at 1 MHz). This study provides a new opportunity to explore and design novel dynamic functional molecular materials.

Author contributions

L. P. M. conceived the project. W. L. prepared the compound. X. B. F. measured and analyzed solid-state NMR spectra. Z. J. X., H. K. L. and Y. F. prepared the samples and performed the DSC, PXRD, TG and dielectric measurements. N. W. observed the evolution of the ferroelastic domain and calculated the spontaneous strain. H. Y. Y. and C. S. contributed to single crystal measurement and analysis. L. P. M. wrote the manuscript, with inputs from all other authors. W. L., N. W. contributed equally.

Conflicts of interest

There are no conflicts to declare.

Acknowledgements

C. S. acknowledges the support from the National Natural Science Foundation of China (Grant No. 22175079). L.-P. M. acknowledges the support from National Natural Science Foundation of China (Grant No. 22205087) and Open Project Program of Jiangxi Provincial Key Laboratory of Functional Molecular Materials Chemistry, Jiangxi University of Science and Technology, (Grant No. 20212BCD42018) and Science and Technology Project of Jiangxi Provincial Department of Education (GJJ210812). H.-Y.Y. acknowledges the support from National Natural Science Foundation of China (Grant No. 21875093 and 22275075) and Natural Science Foundation of Jiangxi Province (Grant No. 20204BCJ22015 and 20202ACBL203001).

References

1 Z. Q. Chu, M. PourhosseiniAsl and S. X. Dong, Review of multi-layered magnetoelectric composite materials and devices applications, *J. Phys. D: Appl. Phys.*, 2018, **51**, 243001.
2 W. B. Li, X. F. Qian and J. Li, Phase transitions in 2D materials, *Nat. Rev. Mater.*, 2021, **6**, 829–846.
3 W. Zhang and R.-G. Xiong, Ferroelectric Metal-Organic Frameworks, *Chem. Rev.*, 2012, **112**, 1163–1195.
4 S. H. Baek, H. W. Jang, C. M. Folkman, Y. L. Li, B. Winchester, J. X. Zhang, Q. He, Y. H. Chu, C. T. Nelson, M. S. Rzchowski, X. Q. Pan, R. Ramesh, L. Q. Chen and C. B. Eom, Ferroelastic switching for nanoscale non-volatile magnetoelectric devices, *Nat. Mater.*, 2010, **9**, 309–314.
5 L. Jin, F. Li and S. J. Zhang, Decoding the Fingerprint of Ferroelectric Loops: Comprehension of the Material Properties and Structures, *J. Am. Ceram. Soc.*, 2014, **97**, 1–27.
6 D. Y. Cong, W. X. Xiong, A. Planes, Y. Ren, L. Manosa, P. Y. Cao, Z. H. Nie, X. M. Sun, Z. Yang, X. F. Hong and Y. D. Wang, Colossal Elastocaloric Effect in Ferroelastic Ni-Mn-Ti Alloys, *Phys. Rev. Lett.*, 2019, **122**, 25–28.
7 S. Kusumoto, Y. Kim and S. Hayami, Flexible metal complex crystals in response to external mechanical stimuli, *Coord. Chem. Rev.*, 2023, **475**, 214890.
8 R. Vlokh and I. Martynyuk-Lototska, Ferroelastic crystals as effective acoustooptic materials, *Ukr. J. Phys. Opt.*, 2009, **10**, 89–99.
9 B. Staskiewicz, I. Turowska-Tyrk, J. Baran, C. Gorecki and Z. Czapla, Structural characterization, thermal, vibrational properties and molecular motions in perovskite-type diaminopropanetetrachlorocadmate $NH_3(CH_2)_3NH_3CdCl_4$ crystal, *J. Phys. Chem. Solids*, 2014, **75**, 1305–1317.
10 W. J. Xu, Z. Y. Du, W. X. Zhang and X. M. Chen, Structural phase transitions in perovskite compounds based on diatomic or multiatomic bridges, *CrystEngComm*, 2016, **18**, 7915–7928.

11 H. Matsuo, Y. Kitanaka, R. Inoue, Y. Noguchi, M. Miyayama, T. Kiguchi and T. J. Konno, Bulk and domain-wall effects in ferroelectric photovoltaics, *Phys. Rev. B*, 2016, **94**, 214111.
12 L.-P. Miao, L.-L. Chu, X.-B. Han, B.-D. Liang, C.-Y. Chai, C.-C. Fan, X.-X. Wang, Y.-F. Yao and W. Zhang, A ferroelastic molecular rotor crystal showing inverse temperature symmetry breaking, *Inorg. Chem. Front.*, 2021, **8**, 2809–2816.
13 Y. Z. Tang, Z. F. Gu, C. S. Yang, B. Wang, Y. H. Tan and H. R. Wen, Unusual Two-step Switchable Dielectric Behaviors and FerroelasticPhase Transition in a Simple 18-Crown-6 Clathrate, *ChemistrySelect*, 2016, **1**, 6772–6776.
14 G. S. Kottas, L. I. Clarke, D. Horinek and J. Michl, Artificial molecular rotors, *Chem. Rev.*, 2005, **105**, 1281–1376.
15 W. Setaka and K. Yamaguchi, Order-Disorder Transition of Dipolar Rotor in a Crystalline Molecular Gyrotop and Its Optical Change, *J. Am. Chem. Soc.*, 2013, **135**, 14560–14563.
16 W. Zhang, H. Y. Ye, R. Graf, H. W. Spiess, Y. F. Yao, R. Q. Zhu and R. G. Xiong, Tunable and Switchable Dielectric Constant in an Amphidynamic Crystal, *J. Am. Chem. Soc.*, 2013, **135**, 5230–5233.
17 X. Zhang, X. D. Shao, S. C. Li, Y. Cai, Y. F. Yao, R. G. Xiong and W. Zhang, Dynamics of a caged imidazolium cation-toward understanding the order-disorder phase transition and the switchable dielectric constant, *ChemComm*, 2015, **51**, 4568–4571.
18 X. G. Chen, Z. X. Zhang, Y. L. Zeng, S. Y. Tang and R. G. Xiong, H/F Substitution induced switchable coordination bonds in a cyano-bridged hybrid double perovskite ferroelastic, *Chem. Commun.*, 2022, **58**, 3059–3062.
19 L. He, P. P. Shi, M. M. Zhao, C. M. Liu, W. Zhang and Q. Ye, Emergent Chirality and Nonlinear Optical Switching in a Ferroelastic Molecular Perovskite Solid Solution, *Chem. Mater.*, 2021, **33**, 799–805.
20 L. He, P. P. Shi, L. Zhou, Z. B. Liu, W. Zhang and Q. Ye, Coexisting Ferroelectric and Ferroelastic Orders in Rare 3D Homochiral Hybrid Bimetal Halides, *Chem. Mater.*, 2021, **33**, 6233–6239.
21 Q. Xu, L. Ye, R. M. Liao, Z. An, C. F. Wang, L. P. Miao, C. Shi, H. Y. Ye and Y. Zhang, H/F Substitution Induced Large Increase of T_c in a 3D Hybrid Rare-Earth Double Perovskite Multifunctional Compound, *Chem. – Eur. J.*, 2022, **28**, e202103913.
22 X. Q. Xu, H. Zhang, X. Q. Huang and Y. L. Liu, A high-temperature halide perovskite molecular ferroelastic with evident dielectric switching, *Inorg. Chem. Front.*, 2021, **8**, 1197–1204.
23 X. Meng, Z.-B. Liu, K. Xu, L. He, Y.-Z. Wang, P.-P. Shi and Q. Ye, Metal regulated organic-inorganic hybrid ferroelastic materials: $[(CH_3)_3CN(CH_3)_2CH_2F]_2MBr_4$ (M = Cd and Zn), *Inorg. Chem. Front.*, 2022, **9**, 1603–1608.
24 R. D. Horansky, L. I. Clarke and J. C. Price, Dielectric response of a dipolar molecular rotor crystal, *Phys. Rev. B: Condens. Matter Mater. Phys.*, 2005, **72**, 014302.
25 T. Akutagawa, H. Koshinaka, D. Sato, S. Takeda, S. I. Noro, H. Takahashi, R. Kumai, Y. Tokura and T. Nakamura, Ferroelectricity and polarity control in solid-state flip-flop supramolecular rotators, *Nat. Mater.*, 2009, **8**, 342–347.
26 Y. Dong, Y. Zhang, X. Li, Y. Feng, H. Zhang and J. Xu, Chiral Perovskites: Promising Materials toward Next-Generation Optoelectronics, *Small*, 2019, **15**, 1902237.
27 B. Saparov and D. B. Mitzi, Organic-Inorganic Perovskites: Structural Versatility for Functional Materials Design, *Chem. Rev.*, 2016, **116**, 4558–4596.
28 J. Jagielski, S. Kumar, W.-Y. Yu and C.-J. Shih, Layer-controlled two-dimensional perovskites: synthesis and optoelectronics, *J. Mater. Chem. C*, 2017, **5**, 5610–5627.
29 K. W. Tao, S. G. Han, C. M. Ji, X. T. Liu, Z. Y. Wu, J. Zhang, J. H. Luo and Z. H. Sun, Structural Phase Transition and Switchable Dielectric Properties of a Unique Two-Dimensional Organic-Inorganic Hybrid Perovskite Compound $(C_6H_{11}NH_2CH_3)_4Pb_3I_{10}$, *Cryst. Growth Des.*, 2018, **18**, 7316–7322.
30 F. Zhang, H. P. Lu, J. H. Tong, J. J. Berry, M. C. Beard and K. Zhu, Advances in two-dimensional organic-inorganic hybrid perovskites, *Energy Environ. Sci.*, 2020, **13**, 1154–1186.
31 W. Li, Z. M. Wang, F. Deschler, S. Gao, R. H. Friend and A. K. Cheetham, Chemically diverse and multifunctional hybrid organic-inorganic perovskites, *Nat. Rev. Mater.*, 2017, **2**, 16099.
32 T. Zhao, C.-C. Chueh, Q. Chen, A. Rajagopal and A. K. Y. Jen, Defect Passivation of Organic-Inorganic Hybrid Perovskites by Diammonium Iodide toward High-Performance Photovoltaic Devices, *ACS Energy Lett.*, 2016, **1**, 757–763.
33 J. C. Blancon, H. Tsai, W. Nie, C. C. Stoumpos, L. Pedesseau, C. Katan, M. Kepenekian, C. M. M. Soe, K. Appavoo, M. Y. Sfeir, S. Tretiak, P. M. Ajayan, M. G. Kanatzidis, J. Even, J. J. Crochet and A. D. Mohite, Extremely efficient internal exciton dissociation through edge states in layered 2D perovskites, *Science*, 2017, **355**, 1288–1291.
34 J. Gong, M. W. Hao, Y. L. Zhang, M. Z. Liu and Y. Y. Zhou, Layered 2D Halide Perovskites beyond the Ruddlesden-Popper Phase: Tailored Interlayer Chemistries for High-Performance Solar Cells, *Angew. Chem., Int. Ed.*, 2022, **61**, e202112022.
35 X. X. Tian, Y. Z. Zhang, R. K. Zheng, D. Wei and J. Q. Liu, Two-dimensional organic-inorganic hybrid Ruddlesden-Popper perovskite materials: preparation, enhanced stability, and applications in photodetection, *Sustainable Energy Fuels*, 2020, **4**, 2087–2113.
36 W. Li, S. Y. Yang, B. L. Guo, X. H. Fu, X. K. Zeng, C. Yan, J. J. Cao, Q. G. Wang and W. Q. Yang, Decoupling excitons behavior of two-dimensional Ruddlesden-Popper PEA_2PbI_4 nanosheets, *J. Alloys Compd.*, 2023, **936**, 168312.
37 Y. Liu, S. G. Han, J. Q. Wang, Y. Ma, W. Q. Guo, X. Y. Huang, J. H. Luo, M. C. Hong and Z. H. Sun, Spacer Cation Alloying of a Homoconformational Carboxylate trans Isomer to Boost in-Plane Ferroelectricity in a 2D Hybrid Perovskite, *J. Am. Chem. Soc.*, 2021, **143**, 2130–2137.

38 G. B. Wu, T. H. Yang, X. Li, N. Ahmad, X. N. Zhang, S. L. Yue, J. Zhou, Y. X. Li, H. Wang, X. H. Shi, S. Z. Liu, K. Zhao, H. Q. Zhou and Y. Zhang, Molecular Engineering for Two-Dimensional Perovskites with Photovoltaic Efficiency Exceeding 18%, *Matter*, 2021, **4**, 582–599.
39 Z. Sun, J. Luo, S. Zhang, C. Ji, L. Zhou, S. Li, F. Deng and M. Hong, Solid-State Reversible Quadratic Nonlinear Optical Molecular Switch with an Exceptionally Large Contrast, *Adv. Mater.*, 2013, **25**, 4159–4163.
40 N. Bloembergen, E. M. Purcell and R. V. Pound, Nuclear magnetic relaxation, *Phys. Rev.*, 1948, **73**, 679–712.
41 T.-J. Yin, K. Xu, L. He, X. Meng, Y. Xu, J.-T. Men, J. Mu, Q. Ye and P.-P. Shi, Templating Influence of Regulated Inorganic Framework in Two-Dimensional Ferroelastic Perovskites: $(C_3H_5CH_2NH_3)_2MCl_4$ (M=Mn and Cd), *Chem. – Eur. J.*, 2023, e202203606.
42 W.-Q. Liao, G.-Q. Mei, H.-Y. Ye, Y.-X. Mei and Y. Zhang, Structural Phase Transitions of a Layered Organic-Inorganic Hybrid Compound: Tetra (cyclopentylammonium) Decachlorotricadmate(II), $(C_5H_9NH_3)_4Cd_3Cl_{10}$, *Inorg. Chem.*, 2014, **53**, 8913–8918.
43 X.-Q. Huang, H. Yu, Z.-K. Xu, T. Gan and Z.-X. Wang, Tuning Dielectric Transitions in Two-Dimensional Organic-Inorganic Hybrid Lead Halide Perovskites, *Inorg. Chem.*, 2021, **60**, 16871–16877.
44 J. Li, Z.-X. Zhang, T. Zhang, P.-Z. Huang, T. Shao, Y. Zhang and D.-W. Fu, Switchable Dielectric Two-Dimensional Lead-Free Perovskite with Reversible Thermochromic Response, *J. Phys. Chem. C*, 2022, 16437–16446.
45 Y. L. Zeng, X. Q. Huang, C. R. Huang, H. Zhang, F. Wang and Z. X. Wang, Unprecedented 2D Homochiral Hybrid Lead-Iodide Perovskite Thermochromic Ferroelectrics with Ferroelastic Switching, *Angew. Chem., Int. Ed.*, 2021, **60**, 10730–10735.
46 Z.-X. Wang, W.-Q. Liao, H.-Y. Ye and Y. Zhang, Sequential structural transitions with distinct dielectric responses in a layered perovskite organic-inorganic hybrid material: $[C_4H_9N]_2[PbBr_4]$, *Dalton Trans.*, 2015, **44**, 20406–20412.
47 C.-R. Huang, X. Luo, X.-G. Chen, X.-J. Song, Z.-X. Zhang and R.-G. Xiong, A multiaxial lead-free two-dimensional organic-inorganic perovskite ferroelectric, *Natl. Sci. Rev.*, 2021, **8**, nwaa232.
48 C.-C. Fan, X.-B. Han, B.-D. Liang, C. Shi, L.-P. Miao, C.-Y. Chai, C.-D. Liu, Q. Ye and W. Zhang, Chiral Rashba Ferroelectrics for Circularly Polarized Light Detection, *Adv. Mater.*, 2022, **34**, 2204119.
49 C.-Y. Su, Y.-F. Yao, Z.-X. Zhang, Y. Wang, M. Chen, P.-Z. Huang, Y. Zhang, W.-C. Qiao and D.-W. Fu, The construction of a two-dimensional organic-inorganic hybrid double perovskite ferroelastic with a high T_c and narrow band gap, *Chem. Sci.*, 2022, **13**, 4794–4800.
50 K. Tao, S. Han, C. Ji, X. Liu, Z. Wu, J. Zhang, J. Luo and Z. Sun, Structural Phase Transition and Switchable Dielectric Properties of a Unique Two-Dimensional Organic-Inorganic Hybrid Perovskite Compound $[C_6H_{11}NH_2CH_3]_4Pb_3I_{10}$, *Cryst. Growth Des.*, 2018, **18**, 7316–7322.
51 S. Wang, L. Li, W. Weng, C. Ji, X. Liu, Z. Sun, W. Lin, M. Hong and J. Luo, Trilayered Lead Chloride Perovskite Ferroelectric Affording Self-Powered Visible-Blind Ultraviolet Photodetection with Large Zero-Bias Photocurrent, *J. Am. Chem. Soc.*, 2020, **142**, 55–59.
52 C. Ji, S. Wang, L. Li, Z. Sun, M. Hong and J. Luo, The First 2D Hybrid Perovskite Ferroelectric Showing Broadband White-Light Emission with High Color Rendering Index, *Adv. Funct. Mater.*, 2019, **29**, 1805038.
53 X.-H. Lv, W.-Q. Liao, P.-F. Li, Z.-X. Wang, C.-Y. Mao and Y. Zhang, Dielectric and photoluminescence properties of a layered perovskite-type organic-inorganic hybrid phase transition compound: $NH_3(CH_2)_5NH_3MnCl_4$, *J. Am. Chem. Soc.*, 2016, **4**, 1881–1885.
54 Z.-Y. Yue, W. Luo, N. Wang, H.-K. Li, Z.-J. Xu, Y. Feng, C. Shi, H.-Y. Ye and L.-P. Miao, Two-dimensional organic-inorganic hybrid perovskite ferroelastics: $(PEA)_2CdCl_4$, $(3\text{-}FPEA)_2CdCl_4$, and $(4\text{-}FPEA)_2CdCl_4$, *CrystEngComm*, 2023, **25**, 1270–1275.
55 D.-F. Li, F. Guo, X.-L. He, Y.-Z. Wu, X.-H. Deng, K.-P. Yang, Y. Sui and Y.-X. Li, A layered hybrid rare-earth double perovskite with two continuous reversible phase transitions induced by unusual two driving gears of fan-like rotation movements, *CrystEngComm*, 2022, **24**, 8496–8502.
56 H.-Y. Zhang, Z.-X. Zhang, X.-G. Chen, X.-J. Song, Y. Zhang and R.-G. Xiong, Large Electrostrictive Coefficient in a Two-Dimensional Hybrid Perovskite Ferroelectric, *J. Am. Chem. Soc.*, 2021, **143**, 1664–1672.
57 C. Shi, L. Ye, Z.-X. Gong, J.-J. Ma, Q.-W. Wang, J.-Y. Jiang, M.-M. Hua, C.-F. Wang, H. Yu, Y. Zhang and H.-Y. Ye, Two-Dimensional Organic-Inorganic Hybrid Rare-Earth Double Perovskite Ferroelectrics, *J. Am. Chem. Soc.*, 2020, **142**, 545–551.
58 W. Wei, H. Gao, M. Fang, Y. Yang, Y. Guan, Y. Wei and Y. Tang, The first 2D organic-inorganic hybrid relaxor-ferroelectric single crystal, *Sci China: Chem.*, 2023, **66**, 466–474.
59 C.-F. Wang, H. Li, M.-G. Li, Y. Cui, X. Son, Q.-W. Wang, J.-Y. Jiang, M.-M. Hua, Q. Xu, K. Zhao, H.-Y. Ye and Y. Zhang, Centimeter-Sized Single Crystals of Two-Dimensional Hybrid Iodide Double Perovskite $(4,4\text{-}Difluoropiperidinium)_4AgBiI_8$ for High-Temperature Ferroelectricity and Efficient X-Ray Detection, *Adv. Funct. Mater.*, 2021, **31**, 2009457.
60 G. C. Psarras, *Greece Dielectric Polymer Materials for High-Density Energy Storage*, William Andrew Publishing, 2018, pp. 11–57.
61 K. Aizu, *J. Phys. Soc. Jpn.*, 1969, **27**, 387–396.
62 S. Park, H. Jeong, Y. Cho, H. Ahn and S.-Y. Jeong, Analysis of the ferroelastic domains and phase transition in the K_2SO_4 crystal, *Phase Transit.*, 2000, **70**, 231–242.

